Microwave Emission and Scattering of Foam Based on Monte Carlo Simulations of Dense Media

Dong Chen, Leung Tsang, *Fellow, IEEE*, Lin Zhou, Steven C. Reising, William E. Asher, Louis Allen Rose, Kung-Hau Ding, *Member, IEEE*, and Chi-Te Chen

***Abstract*—The foam-covered ocean surface is treated as densely packed air bubbles coated with thin layers of seawater. We apply Monte Carlo simulations of solutions of Maxwell's equations to calculate the absorption, scattering, and extinction coefficients at 10.8 and 36.5 GHz. These quantities are then used in dense-media radiative transfer theory to calculate the microwave emissivity. Numerical results of the model are illustrated as a function of foam parameters. Results of emissivities for both horizontal polarization and vertical polarizations at 10.8 and 36.5 GHz are compared with recent experimental measurements.**

***Index Terms*—Dense-media radiative transfer, electromagnetic wave scattering, microwave emissivity, Monte Carlo simulations, ocean foam.**

I. Introduction

TO ESTIMATE the effect of the foam on the ocean surface due to wave breaking on passive microwave remote sensing measurements, various empirical microwave emissivity models have been used [1]–[5]. Williams [1] measured emissivities of foam in a waveguide and found that at X-band, the emissivity of foam depends strongly on the thickness of the foam layer. Wilheit's model [2] treats foam as having neither polarization nor viewing angle dependence. In Pandey's empirical emissivity model [3], the effect of foam was taken into account by coupling of the theoretical expressions of specular ocean surface emissivity with empirical expressions from ocean tower observations and from the analysis of published measurements. Smith [4] measured the brightness temperature of the foam-covered ocean from an aircraft at a 50° incidence angle. He related the emissivities of foam at the three channels (vertical polarization at 19 GHz and both polarizations at 37 GHz) to one another by linear regression. Stogryn [5] used a least squares fit of a polynomial to measurements of artificially generated and naturally occurring foam available as of 1971 and derived an expression for the foam emissivity as a function of incidence angle and frequency. All of these models are empirical fitting procedures using experimental data. The empirical models do not take into account the physical microstructure of foam and the foam layer thickness.

The subject of foam dynamics has attracted great attention. Huang and Jin [6] discussed a composite model of foam scatterers and two-scale wind-driven rough sea surface. Controlled field experiments were performed to measure foam dynamics and the microwave emissivity of calm seawater [7], [8]. Recently, a physically based approach was proposed to model foam as air bubbles coated with seawater [9]. In this approach, wave scattering and emission in a medium consisting of densely packed coated particles are solved using the quasi-crystalline approximation in combination with dense-medium radiative transfer (DMRT) theory [10], [11]. The quasi-crystalline approximation takes into account the effects of dense media, a method that has been verified by controlled laboratory experiments [12], [13].

In this paper, we apply Monte Carlo simulations of solutions of Maxwell's equations of densely packed coated particles to analyze the microwave emission and scattering of foam. The absorption, scattering, and extinction coefficients are calculated. These quantities are then used in DMRT theory to calculate the microwave emissivity. In order to model high-density packing, we use a face-centered-cubic (fcc) structure to place the air bubbles.

In Section II, we describe the physical and geometric properties of foam, both measured and modeled. In Section III, independent scattering results for absorption and scattering are presented. In Section IV, the Monte Carlo simulation and DMRT theory are described. By applying Monte Carlo simulations, we calculate numerical results for absorption rate, scattering rate, and effective permittivity of densely packed air bubbles coated with seawater in a fcc structure. In the Monte Carlo simulations, the volume integral equation is used. The simulation results for emissivity with typical foam parameters at 10.8 and 36.5 GHz are illustrated in Section V. Salient features of the numerical results are 1) the absorption coefficients at 10.8 GHz are appreciable, and 2) the emissivities at 10.8 and 36.5 GHz are comparable. These features are consistent with experimental measurements [8]. Comparisons are also made with experimental measurements [8] for vertical and horizontal polarizations.

Manuscript received August 9, 2002; revised December 4, 2002. This work was supported by the Office of Naval Research under Grant N00014-99-1-0190 to the University of Washington, and the City University of Hong Kong under Grant 9380034. The experimental measurements were also supported by the Office of Naval Research under Award N00014-00-1-280 to the University of Massachusetts, Award N00014-00-0152 to the University of Washington, and Award N0001400WX21032 to the Naval Research Laboratory.

D. Chen is with the Department of Electronic Engineering, City University of Hong Kong, Hong Kong.

L. Tsang is with the Department of Electronic Engineering, City University of Hong Kong, Hong Kong and also with the Department of Electrical Engineering, University of Washington, Seattle, WA 98195 USA (e-mail: eeltsang@cityu.edu.hk).

L. Zhou and W. E. Asher are with the Department of Electrical Engineering, University of Washington, Seattle, WA 98195 USA.

S. C. Reising is with the Microwave Remote Sensing Laboratory, University of Massachusetts at Amherst, Amherst, MA 01003 USA.

L. A. Rose is with the Remote Sensing Division, Naval Research Laboratory, Washington, DC 20375 USA.

K.-H. Ding is with the Air Force Research Laboratory, Hanscom Air Force Base, Bedford, MA 01731 USA.

C.-T. Chen is with the Department of Electrical Engineering, University of Washington, Seattle, WA 98195 USA and is also with the Intel Corporation, Sacramento, CA 95827 USA.

Digital Object Identifier 10.1109/TGRS.2003.810711

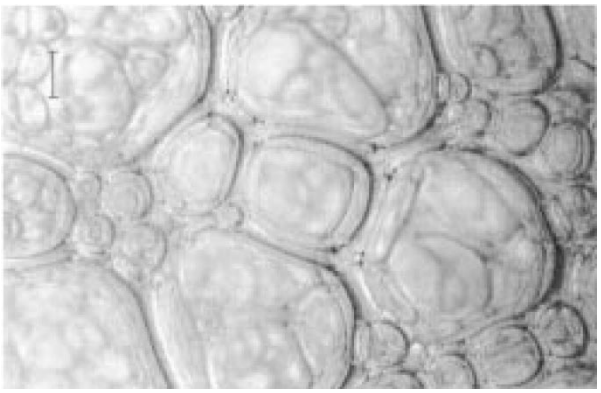

Fig. 1. Video micrograph of artificially generated bubbles in foam on the surface of Chesapeake Bay. The scale in the upper left corner shows a distance of 1 mm.

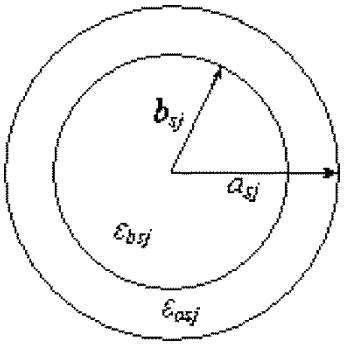

Fig. 2. Spherical dielectric coated particle. a_{sj} and b_{sj} are the outer and inner radii of the spherical shells, respectively. ε_{asj} and ε_{bsj} are permittivities within the shell and in the core of the coated particle, respectively.

II. Description of Foam

A video micrograph of the bubble structure of artificially generated foam on the surface of Chesapeake Bay is shown in Fig. 1. Analysis of this and similar images shows that the void fraction of this foam is 80% to 90% in most cases. To simplify the foam model, it is assumed in this paper that the foam is composed of spherical bubbles. Fig. 2 shows the physical and geometric structure of a spherical dielectric coated particle, where s_j denotes that the coated particle is of the jth species. We assume that there are L species of coated particles in the foam. The core of the coated particle is air, and the shell is seawater. All the particles have the same outer radius, but need not be identical in coating thicknesses. To achieve high density packing, the coated particles are arranged in a fcc structure, as shown in Fig. 3. The particles of the first layer are arranged at point-A; the ones of the second layer are arranged at point-B; the third and fourth layers have the same positions as layer 1 and layer 2, respectively, and so on. The fcc lattice has a fractional volume of $\pi/\sqrt{18} \approx 74\%$ occupied by the particles. The air regions include the core regions of the coated particles and the interstitial space between the coated particles. For example, let N be the number of coated particles, and the jth coated particles be of inner radii b_j and outer radii a_j. The total volume of the foam is V. The fractional volume of coated particles is

$$f = \frac{1}{V}\sum_{j=1}^{N}\frac{4\pi}{3}a_j^3 = 74\%. \tag{1}$$

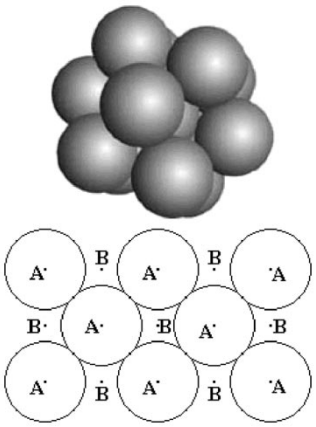

Fig. 3. Three-dimensional graph (upper) and layout (below) of the fcc structure.

The fractional volume of seawater is

$$f_w = \frac{1}{V}\sum_{j=1}^{N}\frac{4\pi}{3}(a_j^3 - b_j^3) = 74\% \cdot \frac{\sum_{j=1}^{N}(a_j^3 - b_j^3)}{\sum_{j=1}^{N}a_j^3}. \tag{2}$$

By choosing values for the inner and outer radii, the foam void fraction $(1.0 - f_w)$ can be on the order of 0.90 (i.e., 90% of the total volume of the foam is air), in agreement with experimental measurements of artificially generated foam [8].

III. Absorption and Extinction Based on Independent Scattering

Let $\overline{E}^e(\overline{r}) = \hat{z}E_z^e(\overline{r})$ be the incident field upon one coated particle. The electric field within the shell at $\overline{r}$ can be written as

$$\overline{E}_{\text{int}}(\overline{r}) = \left[-\hat{z}A + \frac{B}{r^3}\left(\hat{r}2\cos\theta + \hat{\theta}\sin\theta\right)\right]E_z^e(\overline{r}). \tag{3}$$

Similarly, for the case of $\overline{E}^e(\overline{r}) = \hat{x}E_x^e(\overline{r})$ and $\overline{E}^e(\overline{r}) = \hat{y}E_y^e(\overline{r})$ impinging upon the coated particle, by coordinate transformation, the internal field of the coated particle in the shell region can be obtained readily,

$$\overline{E}_{\text{int}}(\overline{r}) = -\hat{x}AE_x^e(\overline{r}) + \frac{B}{r^3}E_x^e(\overline{r}) \cdot \left[\hat{r}2\sin\theta\cos\phi - (\hat{\theta}\cos\theta\cos\phi - \hat{\phi}\sin\phi)\right] \tag{4}$$

$$\overline{E}_{\text{int}}(\overline{r}) = -\hat{y}AE_y^e(\overline{r}) + \frac{B}{r^3}E_y^e(\overline{r}) \cdot \left[\hat{r}2\sin\theta\sin\phi - (\hat{\theta}\cos\theta\sin\phi + \hat{\phi}\cos\phi)\right] \tag{5}$$

where, as shown in the Appendix,

A	$(-3(1+2\varepsilon_r))/((2+\varepsilon_r)(2\varepsilon_r+1)-2b^3(\varepsilon_r-1)^2/a^3)$
B	$(-3(\varepsilon_r-1))b^3/((2+\varepsilon_r)(2\varepsilon_r+1)-2b^3(\varepsilon_r-1)^2/a^3)$
a	outer radius of the coated particle;
b	inner radius of the coated particle;
ε_r	relative permittivity within the shell of the coated particle;
(r,θ,ϕ)	spherical coordinates of $\overline{r}$, $b < r < a$.

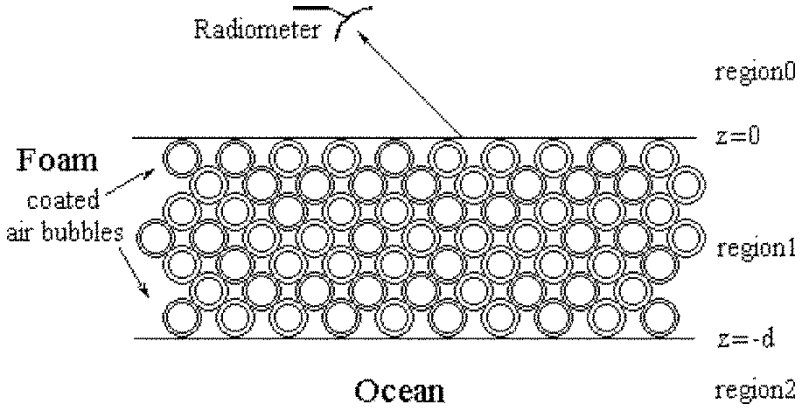

Fig. 4. Geometrical configuration for thermal emission from foam-covered ocean. The foam layer is region 1 and is absorptive and scattering. Region 2 is the ocean.

For the case, $\overline{E}^e(\overline{r}) = \hat{x}E_x^e(\overline{r}) + \hat{y}E_y^e(\overline{r}) + \hat{z}E_z^e(\overline{r})$, the internal field $\overline{E}_{\rm int}(\overline{r})$ at $\overline{r}$ within the shell is the summation of the right sides of (3)–(5).

Assuming the coated particles to be small, the power absorbed by the coated particle is [14, p. 6]

$$\begin{aligned} P_{\rm abs} &= \frac{1}{2}\omega \int_v d\overline{r}\varepsilon_a''(\overline{r}) \left|\overline{E}_{\rm int}(\overline{r})\right|^2 \\ &= \frac{1}{2}\omega\varepsilon_a'' \left(|E_x^e|^2 + \left|E_y^e\right|^2 + |E_z^e|^2\right) \\ &\quad \cdot \left[\frac{4\pi}{3}(a^3 - b^3)\,|A|^2 + \frac{8\pi}{3}\left(\frac{1}{b^3} - \frac{1}{a^3}\right)|B|^2\right] \end{aligned} \quad (6)$$

where

ω angular frequency of exciting field;
ε_a'' imaginary part of permittivity ε_a;
v volume of the coated particle.

The dipole moment $\overline{p}$ of one coated particle can be written as

$$\overline{p} = \int_v d\overline{r}\varepsilon_0(\varepsilon_r - 1)\overline{E}_{\rm int}(\overline{r}). \quad (7)$$

The far field radiated by the dipole $\overline{p}$ in the direction $\hat{k}_s$ is

$$\overline{E}_s = -\frac{k^2 e^{jkr}}{4\pi\varepsilon_0 r}\hat{k}_s \times (\hat{k}_s \times \overline{p}). \quad (8)$$

Consider N coated particles in a volume V. According to the independent scattering assumption, the absorption and scattering of N coated particles is the sum of the individual particles' absorption and scattering

$$\begin{aligned} P_{\rm abs} &= \frac{1}{2}\omega \sum_{j=1}^{N} \int_{v_j} d\overline{r}\varepsilon_{aj}''(\overline{r}) \left|\overline{E}_{\rm int}^j(\overline{r})\right|^2 \\ &= \frac{1}{2}\omega \left(|E_x^e|^2 + \left|E_y^e\right|^2 + |E_z^e|^2\right) \\ &\quad \cdot \sum_{j=1}^{N} \varepsilon_{aj}'' \left[\frac{4\pi}{3}\left(a_j^3 - b_j^3\right)|A_j|^2 \right. \\ &\qquad \left. + \frac{8\pi}{3}\left(\frac{1}{b_j^3} - \frac{1}{a_j^3}\right)|B_j|^2\right] \end{aligned} \quad (9)$$

where

a_j outer radius of coated particle j;
b_j inner radius of coated particle j.

The absorption coefficient is the absorption cross section per unit volume of a collection of particles. It is

$$\begin{aligned} \kappa_{\rm abs} &= \frac{P_{\rm abs}}{\frac{1}{2\eta}\left|\overline{E}^e\right|^2 V} = \frac{\eta\omega}{\left|\overline{E}^e\right|^2 V} \\ &\quad \cdot \sum_{j=1}^{N} \varepsilon_{aj}'' \left[\frac{4\pi}{3}(a_j^3 - b_j^3)\,|A_j|^2 + \frac{8\pi}{3}\left(\frac{1}{b_j^3} - \frac{1}{a_j^3}\right)|B_j|^2\right] \end{aligned} \quad (10)$$

where η is the free-space wave impedance.

The scattering coefficient requires integration of the scattered intensity over all solid angles. It is the scattering cross section per unit volume.

$$\begin{aligned} \kappa_s &= \frac{1}{\left|\overline{E}^e\right|^2 V} \sum_{j=1}^{N} \int_0^{\pi} d\theta \sin\theta \int_0^{2\pi} d\phi r^2 \left|\overline{E}_{sj}\right|^2 \\ &= \frac{1}{V}\sum_{j=1}^{N} \frac{8\pi k^4}{3}|F_j|^2 \end{aligned} \quad (11)$$

where

$$F_j = \frac{(\varepsilon_{rj} - 1)(1 + 2\varepsilon_{rj})(a_j^3 - b_j^3)}{(2 + \varepsilon_{rj})(2\varepsilon_{rj} + 1) - \frac{2b_j^3(\varepsilon_{rj} - 1)^2}{a_j^3}} \quad (12)$$

and ε_{rj} is the relative permittivity of coated particle j.

IV. Monte Carlo Simulations and DMRT Theory

Consider thermal emission from a layered medium with coated particles embedded in a background medium of air, as indicated in Fig. 4. The layer consists of coated particles (region 1), and covers a half space of ocean (region 2). Fig. 5 shows the collection of N coated particles. In the Monte Carlo simulations, we consider the absorption and scattering of N particles collectively by solving Maxwell's equations. The scattering coefficient and absorption coefficient are defined respectively as scattering cross section per unit volume and absorption cross section per unit volume. Thus, we place N

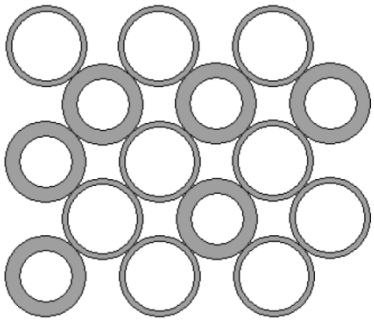

Fig. 5. The collection of N coated particles.

particles in volume V. We calculate the scattering cross section and absorption cross section for these N particles and then divide them by the volume V. These are done for large N and the results of the scattering coefficient and absorption coefficient computed in this manner converge for large N. A volume integral equation is used to solve Maxwell's equations for the N particles. The volume integral equation has the internal electric field in the coated regions as the unknown. Let the incident electric field be impinging upon N coated particles. Coated particle j is centered at $\overline{r}_j$ and has permittivity ε_j. The particles are put in a volume V. Each particle j occupies region V_j, $j = 1, 2, \ldots, N$. Let the internal field in the seawater coating region of particle j be

$$\overline{E}_{\rm int}(\overline{r}) = \overline{E}_j(\overline{r}), \qquad \text{for } \overline{r} \in V_j. \tag{13}$$

The volume integral equation, derived from Maxwell's equations for a collection of particles, is [15]

$$\overline{E}_i(\overline{r}) = \overline{E}^e(\overline{r}) + k^2 \sum_{j=1}^{N} \int_{V_j} d\overline{r}' g(\overline{r}, \overline{r}')(\varepsilon_{rj} - 1)\overline{E}_j(\overline{r}') - \sum_{j=1}^{N} \nabla \int_{V_j} d\overline{r}' \nabla' g(\overline{r}, \overline{r}')(\varepsilon_{rj} - 1)\overline{E}_j(\overline{r}'), \qquad \overline{r} \in V_i \tag{14}$$

where $g(\overline{r}, \overline{r}')$ is the free-space scalar Green's function.

We expand the internal field in the coating region of particle j, $\overline{E}_j(\overline{r})$, into three basis functions. The basis functions are from the electrostatic solutions of the coating region of a coated sphere. The subscript j is suppressed in the following:

$$\overline{E}_j(\overline{r}) = \sum_{\alpha=1}^{3} c_\alpha(\overline{r}) \bar{f}_\alpha(\overline{r}), \quad \overline{r} \in V_j \tag{15}$$

$$\bar{f}_1(\overline{r}) = \frac{1 + 2\varepsilon_r}{3\varepsilon_r}\hat{x} + \frac{1 - \varepsilon_r}{3\varepsilon_r} b^3 \cdot \left[\hat{r}\frac{2}{r^3}\sin\theta\cos\phi - \frac{1}{r^3}(\hat{\theta}\cos\theta\cos\phi - \hat{\phi}\sin\phi)\right] \tag{16a}$$

$$\bar{f}_2(\overline{r}) = \frac{1 + 2\varepsilon_r}{3\varepsilon_r}\hat{y} + \frac{1 - \varepsilon_r}{3\varepsilon_r} b^3 \cdot \left[\hat{r}\frac{2}{r^3}\sin\theta\sin\phi - \frac{1}{r^3}(\hat{\theta}\cos\theta\sin\phi + \hat{\phi}\cos\phi)\right] \tag{16b}$$

$$\bar{f}_3(\overline{r}) = \frac{1 + 2\varepsilon_r}{3\varepsilon_r}\hat{z} + \frac{1 - \varepsilon_r}{3\varepsilon_r} b^3 \left(\hat{r}\frac{2}{r^3}\cos\phi + \hat{\theta}\frac{1}{r^3}\sin\theta\right). \tag{16c}$$

Let

$$\overline{q}_{j\alpha}(\overline{r}) = k^2 \int_{V_j} d\overline{r}' g(\overline{r}, \overline{r}')(\varepsilon_{rj} - 1)\bar{f}_{j\alpha}(\overline{r}') - \nabla \int_{V_j} d\overline{r}' \nabla' g(\overline{r}, \overline{r}')(\varepsilon_{rj} - 1)\bar{f}_{j\alpha}(\overline{r}'). \tag{17}$$

Then the integral equation becomes

$$\sum_{\alpha=1}^{3} c_{i\alpha}\bar{f}_{i\alpha}(\overline{r}) = \overline{E}^e(\overline{r}) + \sum_{\substack{j=1 \\ j\neq i}}^{N}\sum_{\alpha=1}^{3} c_{j\alpha}\overline{q}_{j\alpha}(\overline{r}) + \sum_{\alpha=1}^{3} c_{i\alpha}\overline{q}_{i\alpha}(\overline{r}). \tag{18}$$

We apply the Galerkin method to rewrite (18) into a linear system of equations for the coefficients.

$$\sum_{\alpha=1}^{3} c_{i\alpha} \int_{V_i} d\overline{r}\bar{f}_{i\beta}(\overline{r}) \cdot (\bar{f}_{i\alpha}(\overline{r}) - \overline{q}_{i\alpha}(\overline{r})) = \int_{V_i} d\overline{r}\bar{f}_{i\beta}(\overline{r}) \cdot \overline{E}^e(\overline{r}) + \sum_{\substack{j=1 \\ j\neq i}}^{N}\sum_{\alpha=1}^{3} c_{j\alpha} \int_{V_i} d\overline{r}\bar{f}_{i\beta}(\overline{r}) \cdot \overline{q}_{j\alpha}(\overline{r}) \tag{19}$$

with $i = 1, 2, \ldots, N$ and $\beta = 1, 2, 3$.

Taking the small particle assumption into account, we can make approximations of (19).

$$\sum_{\alpha=1}^{3} c_{i\alpha} \int_{V_i} d\overline{r}\bar{f}_{i\beta}(\overline{r}) \cdot (\bar{f}_{i\alpha}(\overline{r}) - \overline{q}_{i\alpha}(\overline{r})) = \int_{V_i} d\overline{r}\bar{f}_{i\beta}(\overline{r}) \cdot \overline{E}^e(\overline{r}_i) + \sum_{\substack{j=1 \\ j\neq i}}^{N}\sum_{\alpha=1}^{3} k^2(\varepsilon_{rj} - 1)c_{j\alpha} \cdot \int_{V_i} d\overline{r}\bar{f}_{i\beta}(\overline{r}) \cdot \overline{\overline{G}}(\overline{r}_i, \overline{r}_j) \int_{V_j} d\overline{r}'\bar{f}_{j\alpha}(\overline{r}'). \tag{20}$$

After simplifications, (20) can be written as

$$c_{i\beta}K_i = \overline{s}_{i\beta} \cdot \overline{E}^e(\overline{r}_i) + \sum_{\substack{j=1 \\ j\neq i}}^{N}\sum_{\alpha=1}^{3} k^2(\varepsilon_{rj} - 1)c_{j\alpha}\overline{s}_{i\beta} \cdot \overline{\overline{G}}(\overline{r}_i, \overline{r}_j)\overline{s}_{j\alpha} \tag{21}$$

where

$$K_i = \frac{2\varepsilon_{ri} + 1}{3\varepsilon_{ri}} \cdot \frac{1}{9\varepsilon_{ri}} \cdot \frac{4\pi}{3}(a_i^3 - b_i^3) \cdot \left[(2\varepsilon_{ri} + 1)(2 + \varepsilon_{ri}) - \frac{2b_i^3(\varepsilon_{ri} - 1)^2}{a_i^3}\right] \tag{22}$$

$$\overline{s}_{i1} = \int_{V_i} d\overline{r}\bar{f}_{i1}(\overline{r}) = \frac{2\varepsilon_{ri} + 1}{3\varepsilon_{ri}} \cdot \frac{4\pi}{3}(a_i^3 - b_i^3)\hat{x} \tag{23a}$$

$$\overline{s}_{i2} = \int_{V_i} d\overline{r}\bar{f}_{i2}(\overline{r}) = \frac{2\varepsilon_{ri} + 1}{3\varepsilon_{ri}} \cdot \frac{4\pi}{3}(a_i^3 - b_i^3)\hat{y} \tag{23b}$$

$$\overline{s}_{i3} = \int_{V_i} d\overline{r}\bar{f}_{i3}(\overline{r}) = \frac{2\varepsilon_{ri} + 1}{3\varepsilon_{ri}} \cdot \frac{4\pi}{3}(a_i^3 - b_i^3)\hat{z}. \tag{23c}$$

After solving the matrix equations for the coefficients, the power absorbed by N coated particles can be calculated by

$$P_{\rm abs} = \frac{1}{2}\omega \sum_{j=1}^{N} \int_{v_j} d\overline{r}\varepsilon''_{aj}(\overline{r}) \left|\overline{E}_j(\overline{r})\right|^2. \tag{24}$$

The absorption coefficient is

$$\kappa_{\rm abs} = \frac{P_{\rm abs}}{\frac{1}{2\eta}\left|\overline{E}^e\right|^2 V}. \tag{25}$$

The scattered field can be calculated by the following:

$$\overline{E}_s(\overline{r}) = k^2 \sum_{j=1}^{N} \int_{V_j} d\overline{r}' \overline{\overline{G}}(\overline{r},\overline{r}') \cdot (\varepsilon_{rj} - 1)\overline{E}_j(\overline{r}). \tag{26}$$

Taking the result in the far-field, we have

$$\overline{E}_s(\overline{r}) = \frac{k^2 e^{ikr}}{4\pi r}(\hat{v}_s\hat{v}_s + \hat{h}_s\hat{h}_s) \cdot \sum_{j=1}^{N} \int_{V_j} d\overline{r}(\varepsilon_{rj} - 1)\overline{E}_j(\overline{r}) e^{-i\overline{k}_s\cdot\overline{r}_j}. \tag{27}$$

This can be written in terms of the horizontally and vertically polarized components

$$\overline{E}_s(\overline{r}) = (E_{vs}\hat{v}_s + E_{hs}\hat{h}_s)\frac{e^{ikr}}{r}. \tag{28}$$

Then we can obtain the scattered power

$$P_s = \frac{1}{2\eta}\int_0^{2\pi} d\phi_s \int_0^{\pi} d\theta_s \sin\theta_s (|E_{vs}|^2 + |E_{hs}|^2). \tag{29}$$

The scattered power can be decomposed into coherent and incoherent scattered waves [15]. The coherent wave is obtained by averaging the scattered field over the Monte Carlo realizations. To obtain the incoherent power, we have to subtract the coherent intensity. Thus

$$P_s^{\rm inco} = \int_0^{2\pi} d\phi_s \int_0^{\pi} d\theta_s \sin\theta_s \frac{1}{2\eta} \cdot \left\{ \langle |E_{vs} - \langle E_{vs}\rangle|^2\rangle + \langle |E_{hs} - \langle E_{hs}\rangle|^2\rangle \right\} \tag{30}$$

where angular bracket represents averaging over realizations.

The scattering coefficient is

$$\kappa_s = \frac{P_s^{\rm inco}}{\frac{1}{2\eta}\left|\overline{E}^e\right|^2 V} = \int_0^{2\pi} d\phi_s \int_0^{\pi} d\theta_s \sin\theta_s \frac{1}{\left|\overline{E}^e\right|^2 V} \cdot \left\{ \langle |E_{vs} - \langle E_{vs}\rangle|^2\rangle + \langle |E_{hs} - \langle E_{hs}\rangle|^2\rangle \right\}. \tag{31}$$

The extinction coefficient is $\kappa_e = \kappa_s + \kappa_{\rm abs}$ and the albedo is $\varpi = \kappa_s/\kappa_e$. The calculated scattering and absorption coefficients are then substituted into DMRT equations. We also used a Rayleigh phase matrix in the DMRT equations.

The effective permittivity can be calculated as follows. In the forward direction $\overline{k}_s = \overline{k}_i$, the scattered field in the incident polarization can be written as

$$E_s = F\frac{e^{jkr}}{r}. \tag{32}$$

TABLE I
PARAMETERS FOR MONTE CARLO SIMULATIONS SHOWN IN FIGS. 6–10

	a(mm)	b'(mm)	N'	b"(mm)	N"	V(mm³)	f_w (%)
Fig. 6-8	1.0	0.4472	75	0.99795	425	2828	10.5
Fig. 9	0.5	0.2271	75	0.49885	425	353.6	10.5
Fig. 10	0.25	0.1285	75	0.24945	425	44.19	10.5

Then the effective propagation constant is

$$K = {\rm Re}\left(\sqrt{k^2 + \frac{4\pi F}{V}}\right) + j\left(\frac{\kappa_e}{2}\right). \tag{33}$$

The effective permittivity is

$$\varepsilon_{\rm eff} = \frac{K^2}{k^2}. \tag{34}$$

The effective permittivity of foam is used in the Fresnel reflection coefficients for the air-foam interface and the foam-ocean interface in the DMRT theory.

V. NUMERICAL SIMULATIONS OF EMISSIVITY AND COMPARISON WITH EXPERIMENTAL MEASUREMENTS

In the following, we illustrate the numerical results of the emissivity based on a model of coated particles in a fcc structure. The absorption rate, scattering rate, and effective permittivity are first calculated using Monte Carlo simulation. Subsequently, these parameters are used to compute the emissivity. We summarize the foam parameters as follows:

a_j outer radius of coated air bubble j;
b_j inner radius of coated air bubble j;
N number of air bubbles;
V total sample volume in the Monte Carlo simulations;
f_w fractional volume of seawater in foam;
ε_w permittivity of seawater;
θ observation angle.

Note that the permittivity of seawater ε_w is a function of the frequency and other physical parameters such as the temperature and salinity. In our simulations, the permittivities of the seawater at 10.8 and 36.5 GHz are $49.149 + i40.105$ and $13.448 + i24.784$, respectively. In the Monte Carlo simulations, different realizations of the sample of spheres are obtained by rotations of the sample volume. From the results of the different realizations, the coherent fields and the incoherent fields are calculated. The parameters used for Monte Carlo simulations are shown in Table I. The total number of coated air bubbles, which are arranged in a fcc structure, is $N = N' + N'' = 500$. Two species of coated air bubbles are used, as shown in Table I. They have the same outer radii but have different inner radii, b' and b''. We choose N' bubbles randomly of inner radii b', and the rest have inner radii of b''. Seven realizations are generated by rotations of the sample.

The absorption rate, scattering rate, extinction rate, albedo, and effective permittivity calculated from Monte Carlo simu-

TABLE II
NUMERICAL RESULTS FROM MONTE CARLO SIMULATIONS FOR FIGS. 6–8

Parameter	10.8 GHz	36.5 GHz
Absorption rate κ_{abs}	0.2849	0.8854
Scattering rate κ_s	0.01201	0.5738
Extinction rate κ_e	0.2969	1.4592
Albedo	0.04045	0.3933
Effective permittivity	$1.448+i0.158$	$1.158+i0.206$

TABLE III
NUMERICAL RESULTS FROM MONTE CARLO SIMULATIONS FOR FIG. 9

Parameter	10.8 GHz	36.5 GHz
Absorption rate κ_{abs}	0.3009	0.9150
Scattering rate κ_s	2.552×10^{-3}	0.1380
Extinction rate κ_e	0.3035	1.0530
Albedo	8.403×10^{-3}	0.1310
Effective permittivity	$1.508+i0.165$	$1.284+i0.156$

TABLE IV
NUMERICAL RESULTS FROM MONTE CARLO SIMULATIONS FOR FIG. 10

Parameter	10.8 GHz	36.5 GHz
Absorption rate κ_{abs}	0.2686	0.9042
Scattering rate κ_s	6.521×10^{-5}	0.01553
Extinction rate κ_e	0.2686	0.9197
Albedo	2.427×10^{-4}	0.01689
Effective permittivity	$1.478+i0.144$	$1.356+i0.140$

lations for these cases are shown in Tables II–IV, respectively. Next we plot the microwave emissivity dependence on the observation angle at 10.8 and 36.5 GHz for vertical polarization in Fig. 6 and horizontal polarization in Fig. 7. The foam parameters are shown in Table I. As the size of the bubbles increases, the scattering coefficient increases, and the albedo also increases. The increase in albedo causes the corresponding brightness temperatures to decrease.

Next we present the microwave emissivity for vertical polarization and horizontal polarization, at 10.8 and 36.5 GHz, as a function of thickness of the foam layer with different sizes of coated air bubbles, as shown in Figs. 8–10. In actual foam, the air bubbles have a size distribution with mean diameter about 1 mm. However, scattering increases with particle sizes and the effective scattering mean size can be substantially larger than the mean size. In our simulations, we use single size particles. The radii of air bubbles chosen are 1.0, 0.5, and 0.25 mm and represent the effective scattering mean. In actual foam, the coating

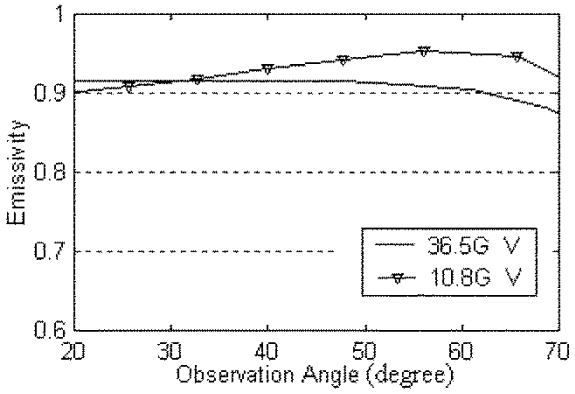

Fig. 6. Emissivity as a function of observation angle for vertical polarization. The radius of the coated air bubble is 1.0 mm.

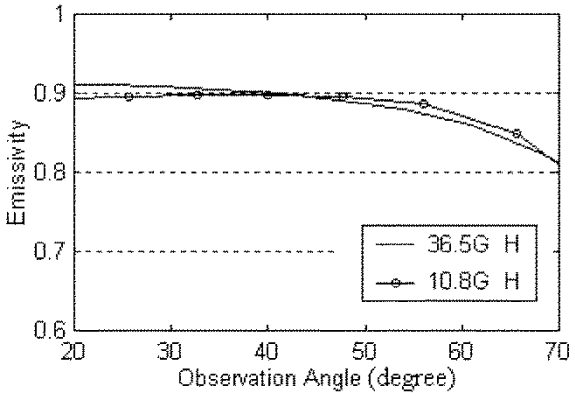

Fig. 7. Emissivity as a function of observation angle for horizontal polarization. The radius of the coated air bubble is 1.0 mm.

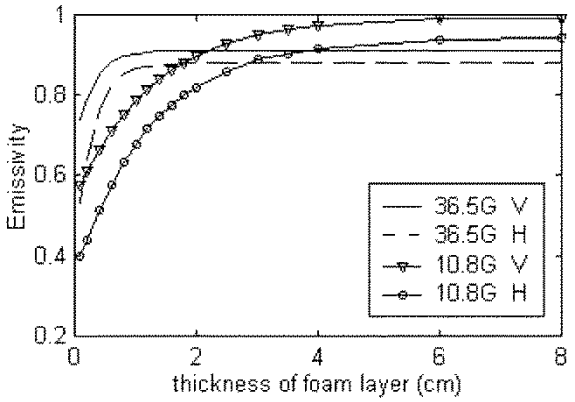

Fig. 8. Emissivity as a function of the thickness of the foam layer at observation angle 53°. The radius of the coated air bubble is 1.0 mm.

thicknesses vary and also vary as a function of depth. For convenience, we have used two coating thicknesses. The observation angle is $\theta = 53^\circ$. From these three figures, we can conclude that as the thickness of the foam layer increases, the emissivity increases correspondingly and then saturates at a particular thickness of the foam layer, for both horizontal polarization and vertical polarization. The saturation point of horizontal polarization is slightly larger than that of vertical polarization. For layer thickness larger than the saturation thickness, the *difference* of emissivity between the two frequencies increases as the size of coated air bubbles increases.

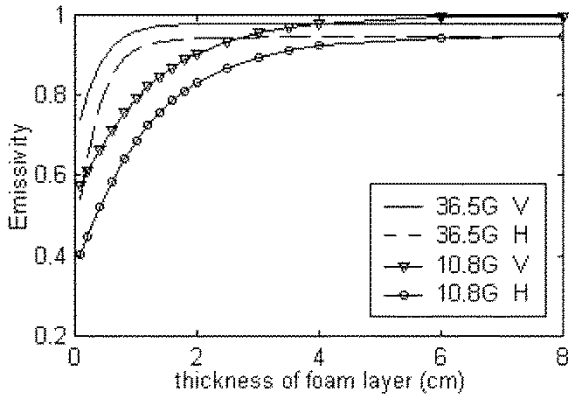

Fig. 9. Emissivity as a function of the thickness of the foam layer at observation angle 53°. The radius of the coated air bubble is 0.5 mm.

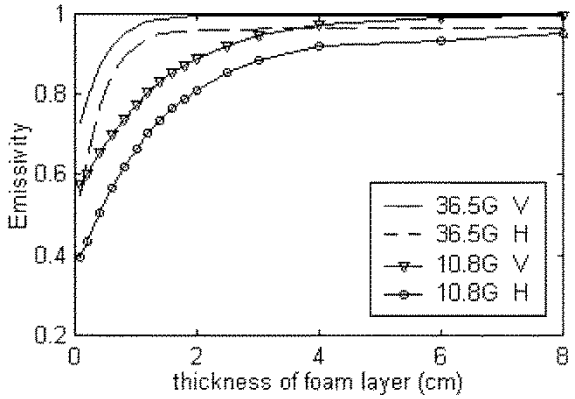

Fig. 10. Emissivity as a function of the thickness of the foam layer at observation angle 53°. The radius of the coated air bubble is 0.25 mm.

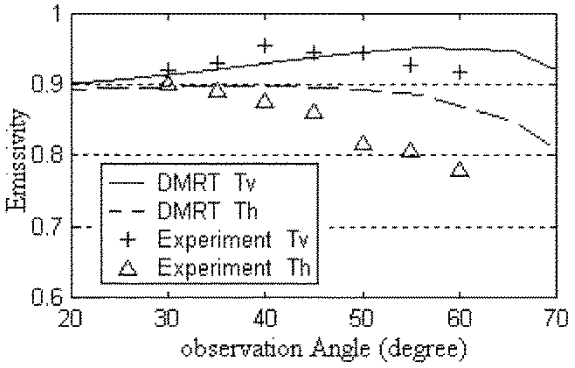

Fig. 11. Comparison between the simulation results and the measurements of the microwave emissivity at 10.8 GHz for horizontal polarization and vertical polarization, respectively.

Next, we compare the microwave emissivity of simulation results with the experimental measurements as a function of observation angle in Figs. 11–12. The parameters used for Monte Carlo simulation are the same as that used in Figs. 6–8, with a coated air bubble radius of 1.0 mm. In the experiment, emissivities of horizontal polarization and vertical polarization were measured at 10.8 and 36.5 GHz, for a foam layer with a mean thickness of 2.8 cm. To facilitate the comparisons, we list in Tables V and VI, the experimental data, the DMRT model results and the air-ocean half space results for the emissivities at

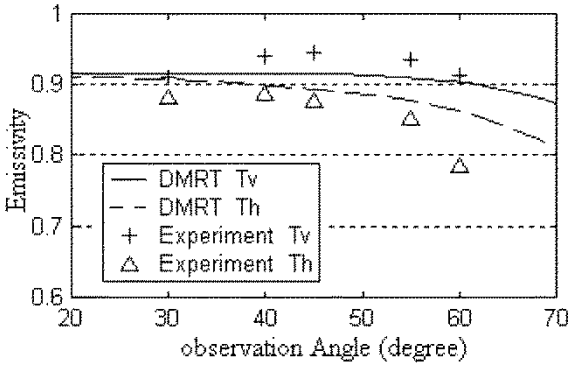

Fig. 12. Comparison between the simulation results and the measurements of the microwave emissivity at 36.5 GHz for horizontal polarization and vertical polarization, respectively.

TABLE V
EMISSIVITIES OF THE EXPERIMENTAL DATA, DMRT MODEL AND AIR–OCEAN HALF SPACE RESULTS AT 10.8 GHZ

$\theta(^\circ)$	Experiment		DMRT model		Air-ocean half space	
	V	H	V	H	V	H
30	0.920	0.900	0.915	0.897	0.422	0.337
35	0.930	0.890	0.923	0.898	0.440	0.322
40	0.955	0.875	0.930	0.899	0.462	0.305
45	0.945	0.860	0.939	0.898	0.489	0.285
50	0.945	0.815	0.946	0.894	0.523	0.263
55	0.929	0.805	0.950	0.885	0.564	0.239
60	0.919	0.780	0.951	0.871	0.615	0.211

TABLE VI
EMISSIVITIES OF THE EXPERIMENTAL DATA, DMRT MODEL AND AIR–OCEAN HALF SPACE RESULTS AT 36.5 GHZ

$\theta(^\circ)$	Experiment		DMRT model		Air-ocean half space	
	V	H	V	H	V	H
30	0.910	0.880	0.916	0.908	0.526	0.429
40	0.940	0.885	0.916	0.900	0.570	0.391
45	0.945	0.875	0.915	0.895	0.599	0.367
55	0.935	0.850	0.911	0.877	0.676	0.310
60	0.912	0.785	0.905	0.863	0.725	0.276

10.8 and 36.5 GHz, respectively. From Figs. 11–12, we see that Monte Carlo simulations produce results in reasonably good agreement with experimental measurements. Both simulations and experiments indicate that absorption at 10.8 GHz is appreciable. In addition, the simulations show that emissivities at 10.8 and 36.5 GHz are comparable. The absorption coefficient at 36.5 GHz is larger than that at 10.8 GHz. However, scattering has a significant effect at 36.5 GHz. The results are in good agreement at small angles of incidence. At large angles, the difference increases. We are presently studying the refinement of the model by investigating realistic foam generation algorithms that can improve the model.

VI. Conclusion

We apply Monte Carlo simulations and dense-media radiative transfer theory to analyze the microwave emissivity and scattering of foam on a seawater surface. We model the foam as densely packed air bubbles with a thin coating of seawater. Numerical simulations show the polarization and frequency dependencies of emissivity on microstructure properties such as foam layer thickness and the size of foam air bubbles. The results of numerical simulations are in good agreement with experimental measurements. In the future, we will study Monte Carlo simulations when there are size and coating thickness distributions. More features, such as two-scale rough sea surface and appropriate structures, can be incorporated into the model in the future. Recently, we have used the second order small perturbation method for rough surface boundary condition for the foam-ocean interface in the DMRT formulation [16].

Appendix
Derivation of Coefficients A/B

Let $\overline{E}_{\rm inc} = \hat{z}E_0$ be the incident field upon one coated particle, as shown in Fig. 2. Assuming the permittivity outside the particle and in the core both to be ε_0, define Φ_1, Φ_2 and Φ_3 are the potentials outside the particle, within the shell and in the core of the coated particle, respectively.

$$\Phi_1 = A_1 r\cos\theta + \frac{B_1\cos\theta}{r^2} \tag{A1}$$

$$\Phi_2 = A_2 r\cos\theta + \frac{B_2\cos\theta}{r^2} \tag{A2}$$

$$\Phi_3 = A_3 r\cos\theta \tag{A3}$$

where r and θ are spherical coordinates.

The boundary conditions are as follows:

$$\Phi_1 = -E_0 r\cos\theta, \quad \text{with } r\to\infty \tag{A4}$$

$$\Phi_1 = \Phi_2, \quad \text{with } r = a \tag{A5}$$

$$\varepsilon_0\frac{\partial\Phi_1}{\partial r} = \varepsilon_a\frac{\partial\Phi_2}{\partial r}, \quad \text{with } r = a \tag{A6}$$

$$\Phi_2 = \Phi_3, \quad \text{with } r = b \tag{A7}$$

$$\varepsilon_a\frac{\partial\Phi_2}{\partial r} = \varepsilon_0\frac{\partial\Phi_3}{\partial r}, \quad \text{with } r = b \tag{A8}$$

where ε_a is the permittivity within the shell.

After solving (A4)–(A8), the coefficients A_2 and B_2 can be written as

$$A_2 = \frac{-3\varepsilon_0(\varepsilon_0+2\varepsilon_a)E_0}{(\varepsilon_0+\varepsilon_a)(2\varepsilon_a+\varepsilon_0) - \frac{2b^3(\varepsilon_a-\varepsilon_0)^2}{a^3}} \tag{A9}$$

and

$$B_2 = \frac{-3\varepsilon_0(\varepsilon_a-\varepsilon_0)b^3E_0}{(2\varepsilon_0+\varepsilon_a)(2\varepsilon_a+\varepsilon_0) - \frac{2b^3(\varepsilon_a-\varepsilon_0)^2}{a^3}}. \tag{A10}$$

The electric field within the shell is

$$\overline{E}_2 = -\nabla\Phi_2 = -\hat{z}A_2 + \frac{B_2}{r^3}\left(\hat{r}2\cos\theta + \hat{\theta}\sin\theta\right). \tag{A11}$$

After some rearrangements, the coefficients A/B in [(3)–(5)] can be obtained from A_2/B_2.

References

[1] G. F. Williams, "Microwave emissivity measurements of bubbles and foam," *IEEE Trans. Geosci. Electron.*, vol. GE-9, pp. 221–224, July 1971.

[2] T. T. Wilheit Jr, "A model for the microwave emissivity of the ocean's surface as a function of wind speed," *IEEE Trans. Geosci. Electron.*, vol. GE-17, pp. 244–249, Apr. 1979.

[3] P. C. Pandey and R. K. Kakar, "An empirical microwave emissivity model for a foam-covered sea," *IEEE J. Oceanic Eng.*, vol. OE-7, no. 3, pp. 135–140, 1982.

[4] P. M. Smith, "The emissivity of sea foam at 19 and 37 GHz," *IEEE Trans. Geosci. Remote Sensing*, vol. 26, pp. 541–547, Sept. 1988.

[5] A. Stogryn, "The emissivity of sea foam at microwave frequencies," *J. Geophys. Res.*, vol. 77, pp. 1658–1666, 1972.

[6] X. Z. Huang and Y. Q. Jin, "Scattering and emission from two-scale randomly rough sea surface with foam scatterers," *Proc. Inst. Elect. Eng. Microwave Antennas Propagat.*, vol. 142, pp. 109–114, Apr. 1995.

[7] W. Asher, Q. Wang, E. C. Monahan, and P. M. Smith, "Estimation of air-sea gas transfer velocities from apparent microwave brightness temperature," *Mar. Technol. Soc. J.*, vol. 32, no. 2, pp. 32–40, 1998.

[8] L. A. Rose, W. E. Asher, S. C. Reising, P. W. Gaiser, K. M. St. Germain, D. J. Dowgiallo, K. A. Horgan, G. Farquharson, and E. J. Knapp, "Radiometric measurements of the microwave emissivity of foam," *IEEE Trans. Geosci. Remote Sensing*, vol. 40, pp. 2619–2625, Dec. 2002.

[9] J. Guo, L. Tsang, W. Asher, K. -H. Ding, and C. -T. Chen, "Applications of dense media radiative transfer theory for passive microwave remote sensing of foam covered ocean," *IEEE Trans. Geosci. Remote Sensing*, vol. 39, pp. 1019–1027, May 2001.

[10] L. Tsang and J. A. Kong, *Scattering of Electromagnetic Waves*. New York: Wiley Interscience, 2001, vol. 3, Advanced Topics, p. 413.

[11] L. Tsang, C.-T. Chen, A. T. C. Chang, J. Guo, and K.-H. Ding, "Dense media relative transfer based on quasicrystalline approximation with applications to passive microwave remote sensing of snow," *Radio Sci.*, vol. 35, no. 3, pp. 731–749, 2000.

[12] A. Ishimaru and Y. Kuga, "Attenuation constant of coherent field in a dense distribution of particles," *J. Opt. Soc. Amer.*, vol. 72, no. 10, pp. 1317–20, 1982.

[13] C. E. Mandt, Y. Kuga, L. Tsang, and A. Ishimaru, "Microwave propagation and scattering in a dense distribution of spherical particles: Experiment and theory," *Waves Random Media*, vol. 2, pp. 225–234, 1992.

[14] L. Tsang, J. A. Kong, and K.-H Ding, *Scattering of Electromagnetic Waves*. New York: Wiley Interscience, vol. 1, Theories and Applications.

[15] L. Tsang and J. A. Kong, *Scattering of Electromagnetic waves*. New York: Wiley Interscience, 2001, vol. 2, Numerical Simulations, pp. 513–517.

[16] L. Zhou, L. Tsang, and D. Chen, "Polarimetric passive microwave remote sensing of wind vectors with foam covered rough ocean surfaces," *Radio Sci.*, submitted for publication.

Dong Chen received the B.Eng. degree in electronic engineering from Fudan University, Shanghai, China, in 1999.

He is currently a Research Assistant with the Department of Electronic Engineering, City University of Hong Kong. His current research interests include numerical computation of electromagnetic wave scattering, propagation in random media and rough surfaces, and fast algorithms in computational electromagnetics.

Leung Tsang (S'73–M'75–SM'85–F'90) was born in Hong Kong. He received the S.B., S.M., and the Ph.D. degrees from the Massachusetts Institute of Technology, Cambridge.

He is currently a Professor of electrical engineering at the University of Washington, Seattle, where he has taught since 1983. Starting September 2001, he has been on leave from the University of Washington and is a Professor Chair and Assistant Head of the Department of Electronic Engineering, the City University of Hong Kong. He is a coauthor of four books: *Theory of Microwave Remote Sensing* (New York: Wiley–Interscience, 1985), *Scattering of Electromagnetic Waves, Vol. 1: Theory and Applications* (New York: Wiley–Interscience, 2000), *Scattering of Electromagnetic Waves, Vol 2: Numerical Simulations* (New York: Wiley–Interscience, 2001), and *Scattering of Electromagnetic Waves, Vol 3: Advanced Topics* (New York: Wiley–Interscience, 2001). His current research interests include wave propagation in random media and rough surfaces, remote sensing, high-speed interconnects, computational electromagnetics, wireless communications, and optoelectronics.

Dr. Tsang was Editor-in-Chief of the IEEE TRANSACTIONS ON GEOSCIENCE AND REMOTE SENSING. He was the Technical Program Chairman of the 1994 IEEE Antennas and Propagation International Symposium and URSI Radio Science Meeting, the Technical Program Chairman of the 1995 Progress in Electromagnetics Research Symposium, and the General Chairman of the 1998 IEEE International Geoscience and Remote Sensing Symposium. He is a Fellow of the Optical Society of America and the recipient of the Outstanding Service Award of the IEEE Geoscience and Remote Sensing Society for 2000. He was also a recipient of the IEEE Third Millennium Medal in 2000. He is also an AdCom member of the IEEE Geoscience and Remote Sensing Society.

Lin Zhou received the B.Eng. and M.Eng. degrees from the University of Electronic Science and Technology of China, Chengdu, China, in 1989, and National University of Singapore in 1999, respectively, both in electronic engineering. He is currently pursuing the Ph.D. degree at the University of Washington, Seattle.

He is currently a Research Assistant with the Department of Electrical Engineering, University of Washington. From 1989 to 1996, he worked in Communication Division, the Civil Aviation Administration of China, Henan, China as an Engineer. His current interests include theoretical and numerical studies of electromagnetic wave scattering and propagation in random media and remote sensing.

Steven C. Reising (S'93–M'98) received the B.S. and M.S. degrees in electrical engineering from Washington University, St. Louis, MO, in 1989 and 1991, respectively. He received the Ph.D. degree from Stanford University, Stanford, CA, in 1998, where his dissertation research focused on low-frequency remote sensing of lightning and its energetic coupling to the ionosphere, producing chemical changes and optical emissions.

Since 1998, he has been an Assistant Professor of electrical and computer engineering at the University of Massachusetts, Amherst. His technical interests include microwave/millimeterwave remote sensing, particularly of the ocean and atmosphere, as well as radiometer design and miniaturization using MMIC architectures. During 1999 and 2000, he was a Navy-ASEE Summer Faculty Fellow at the Naval Research Laboratory, Washington, DC, and he currently serves as a member of the WindSat Science Team. He is the current Editor and past Associate Editor of the IEEE Geoscience and Remote Sensing Society (GRS-S) Newsletter.

Dr. Reising received the URSI/USNC Best Student Paper Prize at the National Radio Science Meeting in Boulder, CO, in 1998. In 2000, he won an Office of Naval Research Young Investigator Award (YIP). He was awarded a Lilly Teaching Fellowship in 2001–2002. He is an ex-officio member of the GRS-S AdCom (without vote). He serves as Chair of the Springfield, MA, Joint Chapter of the IEEE AP, GRS, ED, MTT, and LEO Societies. He is a Member of URSI Commissions F, G, and H, and is the Commission F Co-Chair of the International URSI Working Group on Solar Power Satellites. He is a member of the American Meteorological Society, the American Geophysical Union, Tau Beta Pi, and Eta Kappa Nu.

William E. Asher received the B.A. degree in chemistry from Reed College, Portland, OR, in 1980, and the Ph.D. degree in environmental science and engineering from Oregon Graduate Institute for Science and Technology, Beaverton, OR, in 1987.

His is currently a Senior Oceanographer at the Applied Physics Laboratory, University of Washington, Seattle, and a Staff Scientist at the Department of Environmental Science and Engineering, Oregon Health and Sciences University, Beaverton. His research interests include characterization of breaking waves, air-sea transfer processes, and modeling the formation of secondary organic aerosols. He is an Associate Editor for the *Journal of Geophysical Research Oceans* (American Geophysical Union) and an editor for *Atmospheric Chemistry and Physics* (European Geophysical Society)

Louis Allen Rose (S'60–M'61) received the B.S.E.E. degree from the University of Arkansas, Fayetteville, the M.S. degree in physics from Vanderbilt University, Nashville, TN, and the Ph.D. degree in astrophysics from the University of Minnesota, Minneapolis.

He is currently a Research Physicist in the Microwave Remote Sensing Section, Remote Sensing Division, Naval Research Laboratory (NRL), Washington, DC. He has prepared a set of SSM/I simulator radiometers and has conducted a series of NRL RP-3A aircraft underflight measurements in support of the Navy's initial calibration of the DMSP SSM/I passive microwave sensors. He has performed many field and aircraft experiments to study the emission of microwave radiation from land and water surfaces.

Dr. Rose is a member of the American Astronomical Society and the American Geophysical Union.

Kung-Hau Ding (S'89–M'89) received the B.S. degree in physics from National Tsing-Hua University, Hsinchu, Taiwan. He received the M.S. degrees in physics and electrical engineering and the Ph.D. degree in electrical engineering, in 1989, all from the University of Washington, Seattle, WA.

He is currently a Research Engineer with the Sensors Directorate of the Air Force Research Laboratory, Hanscom Air Force Base, Bedford, MA. From 1989 to 1992, he worked as a Physical Scientist with the Physical Science Laboratory, New Mexico State University, Las Cruces, and from 1993 to 1998, as a Research Scientist with the Research Laboratory of Electronics, Massachusetts Institute of Technology, Cambridge. His research interests include wave propagation and scattering in random media, microwave remote sensing, and radar clutter and target characterizations.

Dr. Ding is a member of the Electromagnetics Academy.

Chi-Te Chen, photograph and biography not available at the time of publication.